PAPER

Facile fabrication of composite cellulose fibrous materials for efficient and consecutive dyeing wastewater treatment†

Dandan Xie,[a] Qiuxia Fu,*[ab] Yue Wang,[a] Jianlong Ge, [ID] [ab] Hailou Wang,[ab] Yu Zhang,[ab] Wei Zhang*[ab] and Haoru Shan [ID] *[ab]

Fabricating dye adsorbents with efficient adsorption properties is of great significance in the treatment of printing and dyeing wastewater. Herein, composite materials of polydopamine decorated cellulose fibrous nonwovens (PDA@CF NWs) were fabricated by constructing a PDA functional layer on the surface of cellulose fibers *via in situ* polymerization. In addition, a three-dimensional adsorbent of 3D PDA@CF NWs with good hydrophilicity, structural stability, and compression resistance could be obtained using a facilely laminating and traditional loop bonding reinforcing technique. Attributed to the efficient and uniform loading of an active PDA functional layer, the resulting PDA@CF NWs exhibited a relatively large adsorption capacity of around 91 mg g^{-1} towards the template dye of methylene blue within a fast equilibrium time of 2 h, which was superior to most of the fibrous adsorbents. In addition, the treatment column of 3D PDA@CF NWs exhibited a breakthrough capacity of 40.9 mg g^{-1}, reaching nearly 50% of the static saturated dye-binding capacity. More importantly, the 3D PDA@CF NWs column could effectively and continuously separate the mixture of different dyes under gravity, highlighting an excellent practical performance. Thus, the PDA@CF NWs are expected to provide a promising candidate for environment-friendly, large-scale and efficient treatment of industrial printing and dyeing wastewater.

Introduction

Nowadays, water pollution caused by organic dyes has become one of the most serious water pollution problems due to the rapid development of the textile and garment industry.[1,2] Organic dye pollutants in wastewater with complex structure, high chroma, strong toxicity, and difficult degradation not only have a certain impact on aquatic organisms but also pose a great threat to human health and survival.[3,4] Up to now, various treatment approaches towards organic dyeing wastewater have been developed, mainly consisting of membrane separation, flocculation, redox, electrochemical, adsorption, *etc*.[5–8] Among these techniques, adsorption has been widely applied in the removal of dyes owing to its remarkable decolorization effect, simple operation, low cost, and wide source of adsorbents.[9,10] Along with the rapid development of adsorption technology, the preparation of green, efficient, and low-cost adsorbents for dyeing wastewater treatment is highly desired.

Compared with the traditional dye adsorbents, such as activated carbon, bentonite, zeolite, ion exchange resin, and chelating resin, fiber-based adsorbents have been widely studied because of their rich sources, abundant types, and easy fabrication.[11,12] Among these fibrous adsorbents, nanofibers have been deemed as a new type of substrate to fabricate dye adsorbents with excellent performance benefitting from their small diameter, high porosity, and unique surface/interface effect.[13,14] Nevertheless, several problems of the nanofiber-based adsorbent still exist, mainly involving relatively low production speed, secondary environmental pollution caused by the use of organic solvent, *etc*.[15] Alternatively, as a type of traditional fibrous product, nonwoven materials have exhibited excellent prospects in the preparation of dyeing wastewater treatment materials due to their advantages of high production efficiency, large output, low cost, superior processability, and structure controllability.[16,17] Up to the present, a series of nonwoven-based adsorbents have been developed. For instance, Haiji *et al.* grafted acrylic acid on the polypropylene nonwovens activated with oxygen plasma, and the modified nonwovens showed high adsorption properties for cationic dyes in organic wastewater.[18] Li *et al.* doped Al into chitosan nonwoven to fabricated dye adsorbent, the resulting Al-doped composite chitosan nonwovens showed improved dye adsorption properties by introducing the chelation interaction between the dye and metal ion center of nonwovens.[19] Although certain progress

aCollege of Textile and Clothing, Nantong University, Nantong, Jiangsu 226019, China. E-mail: fuqx@ntu.edu.cn; zhangwei@ntu.edu.cn; hrshan@ntu.edu.cn

bNational & Local Joint Engineering Research Center of Technical Fiber Composites for Safety and Health, Nantong University, Nantong, Jiangsu 226019, China

† Electronic supplementary information (ESI) available. See https://doi.org/10.1039/d2ra03460c

Paper

has been made in the preparation of nonwovens-based waste-water treatment materials, some bottlenecks of the complex modification process, easy to produce secondary pollution, slow adsorption speed, difficulty to achieve continuous treatment still exist.[20–22] Accordingly, it is highly desired to develop high-performance nonwovens-based adsorbent and thus to realize the continuous dyeing wastewater treatment. Cellulose fibrous nonwovens (CF NWs) possessing characteristics of non-toxicity, excellent permeability, biodegradability, and good biocompatibility, have been widely used in the field of the textile industry.[23,24] Thus, it is expected to fabricate three-dimensional adsorption columns for printing and dyeing wastewater treatment by taking the CF NWs as substrate, nevertheless, no related research has been reported.

Herein, polydopamine decorated CF NWs (PDA@CF NWs) were fabricated *via* the *in situ* polymerization of PDA functional layer on the surface of cellulose fiber, realizing by taking CF NWs as the substrate and dopamine (DA) as the modifier. Additionally, a three-dimensional PDA@CF NWs composite column was designed and constructed by combining the facilely laminating and reinforcing through the traditional nonwoven processing technology of loop bonding, as illustrated in Fig. 1a. Owing to the high-performance PDA coating layer and stable fibrous structure, the composite nonwovens could realize the treatment of dyeing wastewater under static adsorption (Fig. 1b) and dynamic separation (Fig. 1c) patterns. Morphologies and physical/chemical properties of the PDA@CF NWs were regulated mainly by controlling the DA loading amount and polymerization time. Surface wettability, mechanical properties, static and kinetic dye adsorption performance of the PDA@CF NWs were studied. Besides, dynamic breakthrough adsorption and selective separation performance of the 3D PDA@CF NWs were systematically discussed.

Experimental section

Materials

Spunlaced CF NWs were obtained from Zhejiang Furuisen Spunlaced Nonwovens Co., Ltd, China. DA, tris(hydroxymethyl) aminomethane, hydrochloric acid (HCl), sodium chloride (NaCl), methylene blue (MB), and rhodamine B (RhB) were supported by Aladdin Reagent Co., Ltd., China. Methyl orange (MO) was provided by National Medicines Co., Ltd., China. Safranine T (ST) was supplied *via* Shanghai Yien Chemical Technology Co., Ltd, China. Anhydrous ethanol was obtained from Shanghai Linfeng Chemical Reagent Co., Ltd. China.

Fabrication of the PDA@CF NWs

Firstly, the CF NWs were washed with ethanol for 30 minutes at room temperature to remove impurities, and then thoroughly dried in a vacuum oven before use. DA modification solution was obtained by adding dopamine powder at different loading dosages (0, 0.5, 1.0, 2.0, and 3.0 mg mL^{-1}) into 0.05 mol L^{-1} Tris–HCl buffer solution and pH of the Tris–HCl buffer was regulated to 8.5 using 0.1 mol L^{-1} HCl solution. Subsequently, alcohol-washed CF NWs were immersed into DA solution. The *in situ* polymerization of DA on the nonwovens was proceeded under stirring conditions and at room temperature for a period of time (2, 4, 8, and 12 h). Following that, the resulting composite nonwovens were washed with ultrapure water to remove residual chemicals and dried using a vacuum oven at 60 °C for 8 h, thus the PDA@CF NWs prepared with different DA concentrations and modification times were obtained. For preparing the 3D PDA@CF NWs, the resulting composite nonwovens were laminated in multiple layers, and then the layered stacked nonwovens were strengthened by loop bonding technology. Finally, the 3D PDA@CF composite nonwovens with a stable structure were obtained.

Static adsorption performance measurement

In this work, MB was taken as the model cationic dye to perform the dye adsorption performance of the resulting PDA@CF NWs. The initial dye loading dosage was changed from 0 to 70 mg L^{-1}. Meanwhile, the adsorption time was changed from 0 to 12 h. Typically, 3 mg composite nonwovens were immersed into a 6 mL dye solution, and then the mixture was shaken at a constant rate for a designated time. Adsorption capacities of the nonwoven materials were calculated *via* detecting the absorbance intensity changes at 664 nm of the solutions using an ultraviolet-visible (UV-vis) spectrophotometer. The amounts of adsorbed dyes were calculated *via* the following equation:

$$Q_t = \frac{(C_0 - C_t)V}{m} \tag{1}$$

where Q_t represents the binding amount (mg g^{-1}), m represents the amount of PDA@CF NWs (g), C_0 and C_t represent the dye concentration at initial and after adsorption states (mg L^{-1}), and V represents a volume of the dye solution (L).

Dynamic breakthrough adsorption performance measurement

To investigate the dynamic breakthrough performance of the resulting composite nonwovens, 3D PDA@CF NWs by 15 layers of composite nonwovens with a total thickness of about 8 mm were fixed in a homemade plastic filter column with an inner
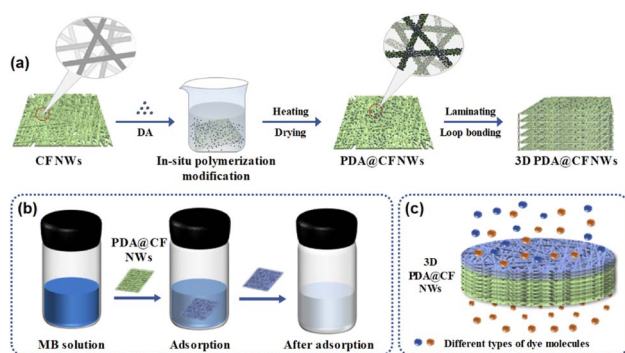

Fig. 1 (a) Schematic illustration of the fabrication process of the *in situ* polymerization, laminating, and loop bonding of the 3D PDA@CF NWs. (b) Static dye adsorption and (c) dynamic dye separation application of the PDA@CF NWs.

diameter of 13 mm. The as-prepared dye solution (taking 50 mg L^{-1} MB solution as an example) was then poured onto the filter column continuously and slowly through the modified nonwovens, following the interaction with the composite materials. And then, the effluent solutions were immediately collected in turn, the volume of the collected solution was controlled at 4 mL at each time. Subsequently, the dye concentration of the collected effluent was calculated *via* the detected UV-vis spectra, and the test was terminated until the absorbance of effluent achieved the initial value of the original dye solution. It is worth pointing out that during the whole process of penetration, the height of liquid level in the filter remained basically and all of the experiments were driven solely by a stable pressure drop of gravity (about 100 Pa).

Selectivity measurement

High selectivity to organic molecules is the key to affecting filtration performance. Thus, it is essential to investigate the selectivity of the as-prepared composite nonwovens by testing the adsorption performances towards different ionic types and molecular sizes of dyes, including cationic dye MB, ST, RhB with different sizes as well as MO was selected as an anionic dye. Herein, the dye filtration experiments were carried out using the above filtration device. As for the mixtures of organic dyes including MB/RhB, MB/ST, and MB/MO, the initial concentration of each dye was controlled at 50 mg L^{-1}. Furthermore, the 3D PDA@CF NWs column was placed in the filtration device, and the dye mixture was filtered under gravity.

Apparatus and characterizations

The morphologies of the relevant composite nonwovens were characterized by utilizing Field emission scanning electron microscopy (FE-SEM, Gemini SEM 300, Carl Zeiss Ltd., Germany). The chemical structure and textural properties of the relevant samples were examined by employing X-ray photoelectron spectroscopy (XPS, K-Alpha+) and Brunauer–Emmett–Teller (BET) analyser (ASAP 2020, Micromeritics Instrument Co., Ltd, USA). The mechanical properties of the original samples and the modified composite nonwovens were measured by using a tensile tester (XJ810, Shanghai XiangJie Instrument Co., Ltd., China). The dynamic water contact angles (WCA) of the relevant nonwovens were determined *via* the SDC-350 contact angle measuring device. The absorbance curves of the dye solutions before and after adsorption were recorded using an ultraviolet spectrophotometer (TU-1810, Beijing Purkinje General Instrument Co., Ltd, China).

Results and discussion

Morphologies, chemical and mechanical properties of the PDA@CF NWs

Firstly, morphology structure of the PDA@CF NWs was investigated and analyzed by FE-SEM, and the resulting representative FE-SEM images of the original substrate and the composite nonwoven modified with various DA concentrations were shown in Fig. 2a–e. As can be seen from Fig. 2a, the initial
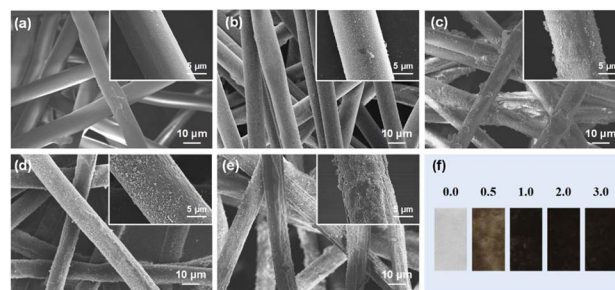

Fig. 2 FE-SEM and the partial enlargement photograph of the PDA@CF NWs fabricated by different DA concentrations of (a) 0, (b) 0.5, (c) 1.0, (d) 2.0, and (e) 3.0 mg mL^{-1}. (f) Optical images of the corresponding PDA@CF NWs.

cellulose nonwoven exhibited a disordered fibrous accumulation structure and relatively smooth fiber surface. After polymerization modification by DA, a rough coating layer could be observed on the surface of cellulose fibers. Moreover, as illustrated in Fig. 2b–e, with the increase of DA concentration, the roughness of the functional layer on the fiber surface gradually enhanced, which might ascribe to the increase of polymerization amount of DA. Fig. 2f shows the optical images of raw nonwovens material and the corresponding PDA@CF NWs. The color of the resulting composite nonwovens gradually darkens with the increase of DA loading concentration.[25] Nevertheless, when the DA concentration was greater than 1.0 mg mL^{-1}, the relevant samples keep dark black and almost had no significant change, indicating that the polymerization modification of DA on nonwovens has reached saturation at the concentration of 1.0 mg mL^{-1}.

In addition to the DA concentration, the polymerization modification time also greatly influences the structure of the PDA@CF NWs. In this work, modification time was controlled at 2, 4, 8, and 12 h under a fixed DA concentration of 1.0 mg mL^{-1}. As showed in the FE-SEM and optical images (Fig. 3a–d), similar to the influences of DA concentration, the functionally loaded substance gradually increased and the color of these PDA@CF NWs also deepened along with the extension of modification time. Obviously, due to the insufficient modification time of 2 h to realize fully polymerization of DA around fibers, thus non-uniform coating layers could be observed on the fiber surface. After modification for 8 h, the load of the PDA functional layer on the surface of the fiber almost reached uniform, indicating that it was almost saturated. Besides, as presented in the SEM-EDS images (Fig. 3e–i), relatively uniformly-distributed C, N, and O elements mapping could be observed on the surface of PDA@CF NWs.[26] The corresponding EDX pattern illustrated a strong signal of N element with a content of 4.5 wt%.

Furthermore, XPS characterization was introduced to confirm the chemical structure of the resultant composite nonwovens. As shown in Fig. 3k, only peaks of C 1s (286.8 eV) and O 1s (532.8 eV) could be detected on the initial CF NWs.[27] After DA polymerization modification, an obvious N 1s peak around 400.08 eV could be observed on the resulting PDA@CF
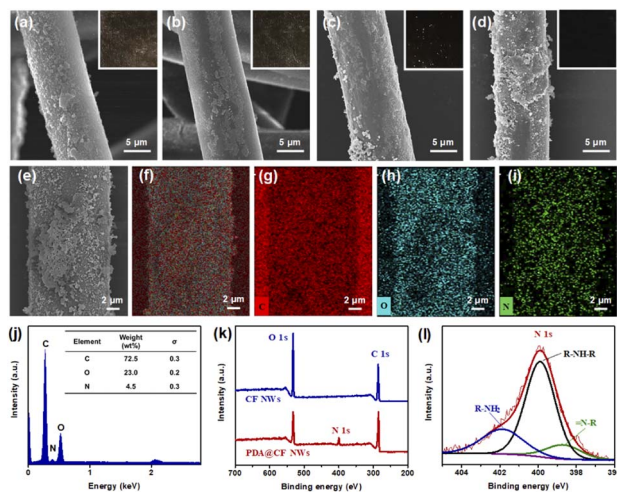
Fig. 3 FE-SEM and the corresponding optical images of the PDA@CF NWs fabricated under different polymerization modification times of (a) 2, (b) 4, (c) 8, (d) 12 h (fixed DA concentration of 1.0 mg mL^{-1}). (e, f) SEM-EDS image, (g–i) SEM-EDS element mapping images, and (j) EDX pattern of the PDA@CF NWs. (k) Survey XPS of the relevant samples. (l) XPS high-resolution N 1s spectra of PDA@CF NWs. (PDA@CF NWs modified by 1.0 mg mL^{-1} DA and 8 h was taken as the representative example to characterize the SEM-EDS and XPS).

Fig. 4 Representative images of the dynamic water permeation process on the surface of (a) CF NWs and (b) PDA@CF NWs. (c) Pictures displaying the compression and recovery process of the 3D PDA@CF NWs. (d) Compression σ−ε curves of the 3D PDA@CF NWs at different compression cycles under a fixed maximum strain of 60%.

NWs. Moreover, the N 1s spectra could be simulated into three peaks at 398.6, 400.1, and 401.8 eV (Fig. 3l), which respectively assigned to tertiary/aromatic amine (=N-R), secondary amine (R-NH-R), and primary amine (R-NH$_2$) functionalities.[28] Moreover, textural properties of the relevant samples were shown in Fig. S1 and Table S1.† Obviously, both of the initial CF NWs and the relevant PDA@CF NWs presented type IV N$_2$ adsorption–desorption isotherms, and the resulting PDA@CF NWs exhibited a relatively larger BET specific surface area of 1.671 m^2 g^{-1} as compared with the original nonwoven substrate (0.841 m^2 g^{-1}), which might ascribe to the effective accumulation of PDA particle on the fiber surface.[29,30] The increased BET surface area was beneficial to the capture and adsorption of dye molecules. Taking the above results into consideration, it could be demonstrated that the functional layer of PDA was successfully grafted onto CF NWs thus endowing the composite PDA@CF NWs with adsorption capability towards dye molecules in the wastewater.

As a new type of dyeing water treatment material, good hydrophilicity and mechanical strength were highly demanded for the 3D PDA@CF NWs. Herein, the influence of PDA coating modification on the surface wettability of the CF NWs was researched by the dynamic wettability test of water droplets. As shown in Fig. 4a and b, after contacting the initial CF NWs, the test water droplet could rapidly infiltrate into the material within about 40 ms due to the excellent hydrophilicity of the cellulose fiber. Although the PDA@CF NWs showed a slightly decreased hydrophilicity due to its relatively larger contact angle and slightly longer infiltration time of 90 ms, the test water droplet also could completely permeate into the resultant composites, declaring its good hydrophilicity and permeability.[31]
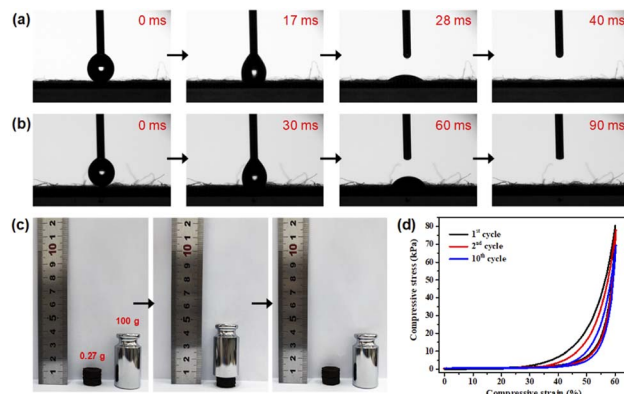
Furthermore, as shown in Fig. S2,† the PDA@CF NWs exhibited a slightly decreased tensile strength (4.11 MPa) than the original CF NWs (4.68 MPa), this might be attributed to the fact that partial mechanical entanglement between cellulose fibers would be destroyed or weakened by the agitation action in the polymerization modification process. Normally, it is worth noting that the sewage treatment columns usually need to bear certain compression and decompression caused by the water pump and water flowing during practical use, thus good compressive mechanical properties are essentially required for the composites of 3D PDA@CF NWs column fabricated by laminating and loop bonding. As displayed in Fig. 4c, the 3D PDA@CF NWs (0.265 g) could be generally restored to their initial shape and size after being pressed by one 100 g weight, illustrating a relatively good mechanical strength. As can be seen from the quantitative compressive stress–strain test results (Fig. 4d), the compressive stress increased slightly when the compressive strain was less than 30%, and then rapidly researched to near 80 kPa as the strain increased to 60%. Despite of the small hysteresis loops, the maximum compressive stress could keep relatively stable in 10 compressive cycles,[32] indicating a good mechanical property of the 3D PDA@CF NWs.

Adsorption performance investigation and optimization of the PDA@CF NWs

The effective loading of PDA endows the synthesized composite materials with effective adsorption and removal capabilities toward organic dye contaminants, mainly rely on the hydrogen bonding interaction, electrostatic adsorption force, together with the π–π stacking interaction between the PDA@CF NWs and these organic pollutants.[33] Generally, the PDA contents on nonwovens remarkably affected the dye adsorption performance of the PDA@CF NWs, which mainly depended on the initial DA concentration and polymerization deposition time. Results of the effect of DA loading on adsorption capacity of the composite nonwovens were displayed in Fig. 5a and b. With the
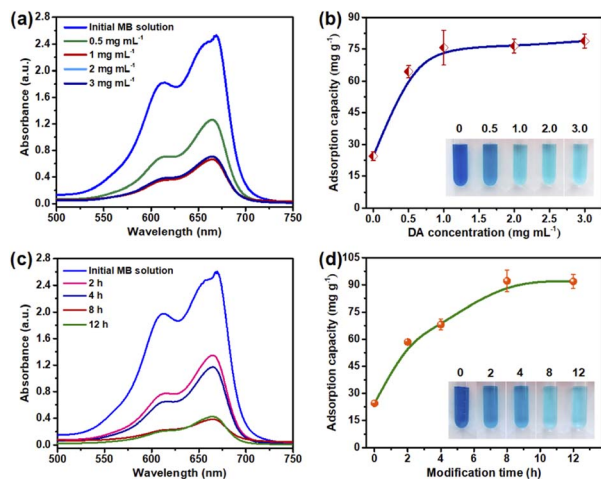
Fig. 5 Spectrum and MB adsorption capacity of the PDA@CF NWs fabricated by (a, b) different DA concentrations and (c, d) different polymerization modification time. The insets show the colors of MB solution and the corresponding effluent.
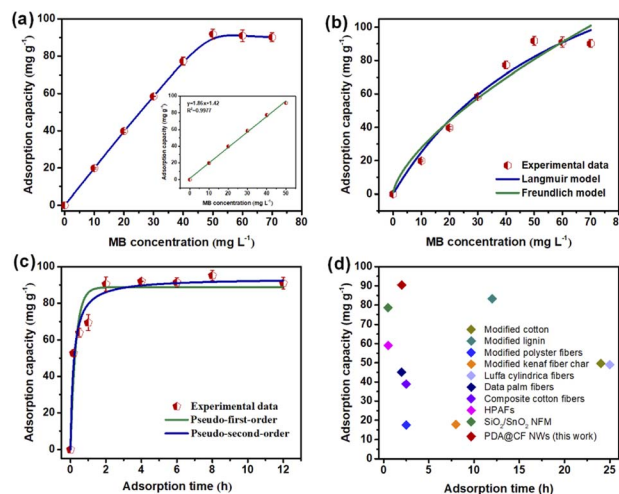

Fig. 6 (a) Adsorption capacities and (b) isothermal adsorption simulation of the PDA@CF NWs at different initial concentrations. (c) Influence of adsorption time on the adsorption capacity and the relevant adsorption kinetics analysis of the PDA@CF NWs. (d) Performance comparison of the PDA@CF NWs to these dye adsorption materials. The inset in (a) exhibits the linear fitting relationship between the adsorption capacity and initial MB concentration ranging from 0 to 50 mg L^{-1}.

increase of DA loading dosage (from 0 to 1.0 mg mL^{-1}), the MB adsorption capability of the resulting PDA@CF NWs was improved rapidly from 22.4 to 75.7 mg g^{-1}. This may be ascribed to the gradually completing of the PDA functional layers and thus the dramatical increasing of adsorption activated sites on the surface of cellulose fibers.[34] Following that, the composite nonwovens keep an almost unchanged adsorption capability with the further increasing DA concentration, which might due to the saturation of the PDA deposition.

Moreover, as demonstrated in Fig. 5c and d, the effect of polymerization deposition time on the performance of PDA@CF NWs was investigated. Similarly, with the increment of polymerization deposition time, MB adsorption capacity also gradually increased to almost 91 mg g^{-1}. After the modification time was longer than 8 h, the resulting composite nonwovens presented an equilibrium adsorption capacity. This is mainly because the available adsorption sites could be gradually occupied by the dye molecules at the initial adsorption stage, thus leading to a continuous improvement in the adsorption capacity. Following that, with the progress of adsorption, the active sites on the functional PDA layer were gradually consumed, and the adsorption amounts reached equilibrium.[33] Thus PDA@CF NWs fabricated from the optimum modification parameters including DA concentration of 1.0 mg mL^{-1} and modification time of 8 h were taken as the representative sample to conduct the following adsorption experiments.

In this work, the effects of dye concentration on the performance of PDA@CF NWs were comprehensively evaluated via testing the adsorption equilibrium uptakes under different initial MB concentrations ranging from 0 to 70 mg L^{-1}. As the MB concentrations raised from 0 to 40 mg L^{-1}, the adsorption capacity of the PDA@CF NWs almost exhibited a linear positive correlation with the MB concentration at a high linear coefficient of 0.9977 (inset of Fig. 6a). And the composite nonwovens keep a saturated MB adsorption capability of 91.83 mg g^{-1} with the further increasing of MB concentrations. Generally,

traditional Freundlich and Langmuir isothermal adsorption models were introduced to quantitatively investigate the isothermal dye adsorption processes of the PDA@CF NWs, that are respectively expressed as follows:[33,34]

$$\text{Freundlich model}: \ \lg q_e = \frac{\lg C_e}{n} + \lg K_F \tag{2}$$

$$\text{Langmuir model}: \ \frac{1}{q_e} = \frac{1}{q_{max}} + \frac{1}{K_a q_{max} C_e} \tag{3}$$

where q_e is the equilibrium adsorption capacity under different initial concentrations of MB solution (mg g^{-1}), q_{max} represents the maximum adsorption capability (mg g^{-1}), C_e represents the MB concentration at equilibrium adsorption state (mg L^{-1}), K_F and K_a are equilibrium constant of Freundlich and Langmuir models, respectively, n is the adsorption strength constant. The resultant fitting curves and calculated parameters are presented in Fig. 6b and Table 1. As can be seen from the correlation coefficient (R^2) shown in Table 1, the adsorption isothermal process of PDA@CF NWs was more described suitably through the Langmuir model ($R^2 = 0.942$), confirming homogeneous monolayer adsorption occurred on the surface of composite nonwovens.[35] More interestingly, the theoretical maximum

Table 1 Langmuir and Freundlich adsorption isotherms parameters for MB adsorption by PDA@CF NWs

Langmuir adsorption model			Freundlich adsorption model		
q_{max} (mg g^{-1})	K_a (L mg^{-1})	R^2	K_F	$1/n$	R^2
191.341	0.015	0.942	6.011	0.664	0.907

amount calculated based on the Langmuir model was assigned to 191.341 mg g^{-1}, further indicating the relatively high adsorption capacity towards MB.

Furthermore, to further quantitatively evaluate the dye adsorption performance of the resulting composite nonwovens, the kinetic adsorption performance of the PDA@CF NWs was extensively investigated *via* detecting the binding capacity of adsorbed dye at gradually increasing contact time (0, 0.2, 0.5, 1, 2, 4, 6, 8, and 12 h), as displayed in Fig. 6c. Significantly, the adsorption capacity of the PDA@CF NWs increased sharply and then approached the equilibrium value of 91 mg g^{-1} within 2 h, demonstrating the efficient and rapid capturing capability of the composite nonwovens towards MB. Moreover, to further evaluate the type of adsorption force between PDA@CF NWs and MB molecules, we employed the pseudo-first and second-order kinetic models to analyze these resulting dynamic adsorption results:[36,37]

$$\text{Pseudo-first-order model}: \quad q_t = q_e\left(1 - \frac{1}{e^{k_1 t}}\right) \quad (4)$$

$$\text{Pseudo-second-order model}: \quad q_t = \frac{k_2 q_e^2 t}{1 + k_2 q_e t} \quad (5)$$

where q_t is the adsorption capacity at relevant adsorption time (mg g^{-1}), q_e is the equilibrium adsorption capacity of MB solution (mg g^{-1}), k_1 and k_2 are the rate constants of the two models, respectively. The resultant fitting curves and calculated parameters, shown in Fig. 6c and Table 2, revealed that the pseudo-second-order model was followed much well for describing the adsorption results as confirmed by the higher correlation coefficients ($R^2 = 0.968$) compared to another model ($R^2 = 0.911$). Overall, it was demonstrated that the dye adsorption performance endows the as-prepared PDA@CF NWs with a high potential to construct packing columns for the practical separation of dyes in the future. Moreover, taking the relatively high adsorption capability (almost 91 mg g^{-1}) and short equilibrium time (2 h) into consideration, the PDA@CF NWs exhibited a relatively superior comprehensive performance over a range of fibrous dye adsorbents (Fig. 6d and Table S2†),[38–47] highlighting its great potential in the practical printing and dyeing wastewater treatment.

Dynamic breakthrough and separation performance of the 3D PDA@CF NWs

Since the aim of this work is to develop a high-efficiency dye adsorbent to realize effective and continuous dyeing water treatment, thus it is of great importance to evaluate the practical performance of the resulting composite nonwovens.[48] Firstly, the dynamic breakthrough adsorption capability of PDA@CF

NWs that greatly influences the dyeing water treatment rate and flux was measured. Herein, cylindrical nonwoven columns with a thickness of about 8 mm that laminated and loop-bonded by 3D PDA@CF NWs were filled in the plastic filter to purify MB solution (50 mg L^{-1}) to conduct the measurement and calculation of dynamic MB adsorption capacity. As presented in the corresponding photographs (Fig. 7a), after flowing through the nonwoven columns driven by its gravity, the dark blue dyeing wastewater simulated solution transformed to relatively clean water without obvious dye pollutant, exhibiting a fast dynamic adsorption rate. By quantitatively analyzing the whole dynamic adsorption process, a typical adsorption breakthrough curve was observed. As displayed in Fig. 7b, the absorbance of the effluent rose slowly and then reached the value of the initial MB solution at the outlet volume of 440 mL. According to the calculation results, 10%, 50%, and 100% dynamic breakthrough binding capacity of the 3D PDA@CF NWs column was almost 11, 28, and 40.9 mg g^{-1}, respectively, nearly reaching 12%, 31% and 50% of the static saturated capacity (91 mg g^{-1}). The unsatisfactory dynamic breakthrough capacity of the composite nonwovens might be attributable to the relatively large and non-uniform pore size large fiber diameter caused by the relatively large diameter, as well as the small packing thickness of the 3D PDA@CF NWs.[49,50] On the one hand, the large pore size is beneficial to the rapid mass transfer and diffusion of the dye molecules in the nonwoven materials and the rapid flow of the dyeing water simulated water; on the other hand, the synthetic action of rapid diffusion and solution flow would result in the insufficient contact of dye molecules with the adsorption ligands on the fiber surface, eventually leading to the relatively poor dynamic breakthrough capacity. However, these shortcomings could be improved by optimizing the
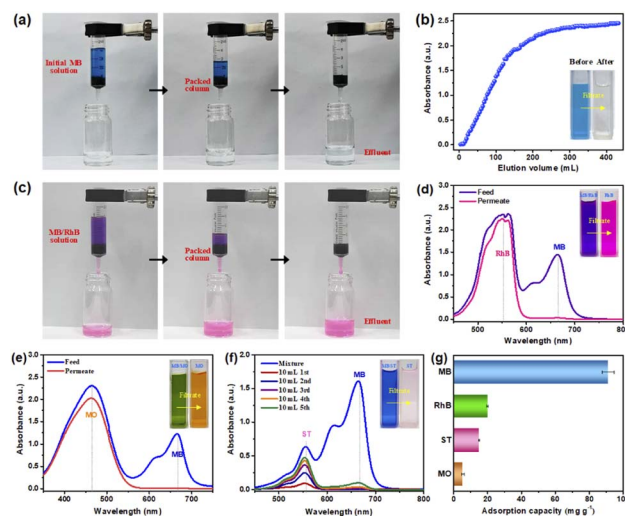

Fig. 7 (a) Photographs showing the dynamic MB removal processes of the 3D PDA@CF NWs and (b) the corresponding breakthrough curve. (c) Photographs exhibiting the dynamic MB/RhB selective separation processes. The UV-Vis spectra of (d) MB/RhB, (e) MB/MO, and (f) MB/ST before and after filtration by the PDA@CF NWs packed column. (g) The different adsorption capacities of the PDA@CF NWs towards MB, ST, MO, and RhB.

Table 2 Pseudo-first and second order kinetic parameters of MB by PDA@CF NWs

Pseudo-first-order model			Pseudo-second-order model		
q_e (mg g^{-1})	K_1 (min^{-1})	R^2	q_e (mg g^{-1})	K_2 (min^{-1})	R^2
88.709	3.384	0.911	93.142	0.059	0.968

microstructure, laminating, and loop-bonding structure of the 3D PDA@CF NWs as well as the corresponding application parameters, *etc.*[51] Fortunately, the dynamic MB removal experiment was conducted solely drove by the MB solution at a constant height of 10 mm, equal to the driving pressure of 100 Pa, highlighting its great practical application potential in the field of high-throughput dyeing wastewater treatment.

Generally, various kinds of dyes usually are used simultaneously in the printing and dyeing industry production, thus good adsorption selectivity is also highly required for the dye adsorbents.[52] As shown in Fig. 7c, the initial MB/RhB mixture exhibits a color of purple, after flowing through and separating by the PDA@CF NWs column under the gravity driving of the simulated dyeing water itself (about 100 Pa), the filtrate (first 10 mL) exhibited a significant color of rose-red of the pure RhB solution. By further characterizing absorbance of the feed and permeate solution, it could be found that the characteristic peak of MB (665 nm) was disappeared as compared with the initial feed mixture, only a strong peak around 552 nm of RhB was observed in the filtrate solution (Fig. 7d), indicating the highly-efficient separation of the 3D composite nonwovens towards MB from the mixture of MB/RhB. Similarly, as presented in Fig. 7e, after the MB/MO mixture passed through the composite nonwoven column, the color of the filtrate (initial 10 mL) changed suddenly from green to orange of MO, and the absorbance spectra also almost changed from double peaks to the single peak of MO, which is consistent with the phenomenon of MB/RhB. Whereas, different from the MB/RhB and MB/MO, a weak peak around 552 nm of ST could be observed in the first 10 mL filtrate of the MB/ST (Fig. 7f). With the further increase of filtrate volume, the characteristic absorption peak of ST gradually strengthened along with a slightly increased MB characteristic peak, demonstrating a relatively poor selective separation property of PDA@CF NWs towards MB and ST.

To further indicate the intrinsic factor of differential separation capability of the PDA@CF NWs column, the saturated static adsorption capability tests towards these different dyes were carried out. As exhibited in Fig. 7g, saturated adsorption capacities of the PDA@CF NWs towards RhB, ST, and MO were 19.9, 14.9, and 5.4 mg g^{-1}, respectively, which significantly lower than the MB (91 mg g^{-1}). The differential adsorption capacity could ascribe to the difference of molecular weight and the ionic types (surface charge) of these organic dyes.[40,53] On the one hand, the MB possesses the minimal molecular weight (319.85 g mol^{-1}) thus a little three-dimensional volume among these template dyes, which is in the order of MB < ST (350.84 g mol^{-1}) < RhB (479.01 g mol^{-1}). On the other hand, the negatively charged surface of anionic MO dye makes it difficult to be adsorbed by the negatively charged PDA on the fiber surface at neutral pH. Accordingly, the above results demonstrate the relatively specific selectivity of the PDA@CF NWs towards MB.

Furthermore, durability is critical for evaluating the practical use performance of the composite nonwoven materials, which needs to be systematically investigated. Herein, durability of the PDA@CF NWs was evaluated by testing the cycle adsorption performance, which was conducted by taking NaCl solution (1 M) as the eluent for MB desorption. As can been seen from Fig. S3a.†, the PDA@CF NWs presented a reduced regeneration efficiency with increasing cycle numbers. This might ascribe to the fact that a part of MB molecules might cannot be desorbed from the membranes by NaCl solution, and a slight weight loss of the composite still exist in the regeneration processes, thereby resulting in the decreased regeneration efficiency. Whereas, regeneration efficiency of the PDA@CF NWs still could remain above 70% after five cycles.[33] Additionally, the PDA@CF NWs also presented dark black color after five adsorption–desorption cycles, and obvious PDA coating layer could be observed on the fiber surface (Fig. S3b†), demonstrating the relatively stable structure of the PDA@CF NWs. Moreover, in addition to the removal of dye pollutants and the corresponding reduction of chemical oxygen demand (COD), the resultant synthesized materials also exhibited certain adsorption capability towards antibiotic pollutants including ciprofloxacin and levofloxacin (Fig. S4†), illustrating the great potential of PDA@CF NWs in the treatment of other organic pollutants in industrial wastewater.

Conclusions

In summary, a new-type, efficient, and environmental-friendly composite nonwoven-based dye adsorbent of PDA@CF NWs was developed by combining *in situ* polymerization, laminating, and reinforcing through the traditional nonwoven processing technology of loop bonding. The surface physical and chemical structure of the composite nonwoven was optimized by regulating the DA loading amount and modification time. The resulting 3D PDA@CF NWs exhibited good hydrophilicity, structural stability, and compression resistance. Due to the effective PDA functional coating layer and good pore connectivity of nonwoven, the resulting composite material showed relatively large static saturated and dynamic breakthrough capacities of 91 and 40.9 mg g^{-1} towards the template dye MB, respectively. Moreover, the 3D PDA@CF NWs columns could effectively and continuously separate different dye mixtures under a small gravity driving of 100 Pa due to its unique adsorption selectivity, highlighting an excellent practical performance. Considering the simple fabrication process, stable and controllable structure, good adsorption, and separation properties, we sincerely believe that this novel PDA@CF NWs would provide a kind of functional materials for the rapid, environment-friendly, efficient adsorption and separation of dyes, and can be also further applied to metal ion adsorption, water filtration, *etc.*

Conflicts of interest

There are no conflicts to declare.

Acknowledgements

Notes and references

1 C. C. Allègre, P. Moulin, M. Maisseu and F. Charbit, Treatment and reuse of reactive dyeing effluents, *J. Membrane Sci.*, 2006, **269**, 15–34.

2 P. A. Soares, T. F. C. V. Silva, D. R. Manenti, S. M. A. G. U. Souza, R. A. R. Boaventura and V. J. P. Vilar, Insights into real cotton-textile dyeing wastewater treatment using solar advanced oxidation processes, *Environ. Sci. Pollut. Res.*, 2014, **21**, 932–945.

3 F. Uddin, Environmental hazard in textile dyeing wastewater from local textile industry, *Cellulose*, 2021, **28**, 10715–10739.

4 J. A. S. Vendemiatti, N. G. Camparotto, C. Vidal, J. Cristale, E. V. D. Agapito, A. C. Oliveira, E. A. Rodrigues, C. C. Montagner, G. A. Umbuzeiro and P. Prediger, New benzotriazoles generated during textile dyeing process: Synthesis, hazard, water occurrence and aquatic risk assessment, *J. Hazard. Mater.*, 2020, **403**, 123732.

5 Y. Tian, B. Z. Ju, S. F. Zhang and L. N. Hou, Thermoresponsive cellulose ether and its flocculation behavior for organic dye removal, *Carbohyd. Polym.*, 2016, **136**, 1209–1217.

6 Y. Liu, F. R. Zhang, W. X. Zhu, D. Su, Z. Y. Sang, X. Yan, S. Li, J. Liang and S. X. Dou, A multifunctional hierarchical porous SiO$_2$/GO membrane for high efficiency oil/water separation and dye removal, *Carbon*, 2020, **160**, 88–97.

7 O. Gercel, Removal of textile dye from aqueous solution by electrochemical method, *Sep. Sci. Technol.*, 2016, **51**, 711–717.

8 T. Li, X. L. Yang, H. L. Song, H. Xu and Q. L. Chen, Quinones contained in wastewater as redox mediators for the synergistic removal of azo dye in microbial fuel cells, *J. Environ. Manage.*, 2022, **301**, 113924.

9 L. Bulgariu, L. Belen Escudero, O. S. Bello, M. Iqbal, J. Nisar, K. A. Adegoke, F. Alakhras, M. Kornaros and I. Anastopoulos, The utilization of leaf-based adsorbents for dyes removal: A review, *J. Mol. Liq.*, 2019, **276**, 728–747.

10 W. Li, B. N. Mu and Y. Q. Yang, Feasibility of industrial-scale treatment of dye wastewater *via* bio-adsorption technology, *Bioresour. Technol.*, 2019, **277**, 157–170.

11 Y. Li, H. N. Xiao, M. D. Chen, Z. P. Song and Y. Zhao, Absorbents based on maleic anhydride-modified cellulose fibers/diatomite for dye removal, *J. Mater. Sci.*, 2014, **49**, 6696–6704.

12 G. Crini, Non-conventional low-cost adsorbents for dye removal: A review, *Bioresource Technol.*, 2019, **277**, 157–170.

13 D. N. Phan, M. Q. Khan, N. T. Nguyen, T. T. Phan, A. Ullah, M. Khatri, N. N. Kien and I. S. Kim, A review on the fabrication of several carbohydrate polymers into nanofibrous structures using electrospinning for removal of metal ions and dyes, *Carbohyd. Polym.*, 2021, **252**, 117175.

14 J. J. Xue, T. Wu, Y. Q. Dai and Y. N. Xia, Electrospinning and electrospun nanofibers: Methods, materials, and applications, *Chem. Rev.*, 2019, **119**, 5298–5415.

15 B. Zhang, X. Yan, H. W. He, M. Yu, X. Ning and Y. Z. Long, Solvent-free electrospinning: Opportunities and challenges, *Polym. Chem*, 2017, **8**, 333–352.

16 T. Demirel, Y. Yavuz, M. E. Ureyen and A. S. Koparal, Investigation of adsorption behavior of cationic nonwoven textiles as an alternative and environmentally friendly adsorbent to remove the Reactive blue 21 dye from a model solution, *Desalin. Water Treat.*, 2021, **242**, 304–315.

17 Y. Kiyak, B. Maze and B. Pourdeyhimi, Microfiber nonwovens as potential membranes, *Sep. Purif. Rev.*, 2019, **48**, 282–297.

18 A. Haji and M. S. Shoushtari, Grafting of poly (propylene imine) dendrimer on polypropylene nonwoven: Preparation optimization, characterization, and application, *Fibers Polym.*, 2019, **20**, 913–921.

19 S. Li, J. Y. ang, S. Rashid, C. S. Shen and J. S. Liu, Al-doped chitosan nonwoven in a novel adsorption reactor with a cylindrical sleeve for dye removal: Performance and mechanism of action, *RSC Adv.*, 2016, **6**, 110935–110942.

20 D. C. Wang, X. G. Yang, H. Y. Yu, J. P. Gu, D. M. Qi, J. M. Yao and Q. Q. Ni, Smart nonwoven fabric with reversibly dual-stimuli responsive wettability for intelligent oil-water separation and pollutants removal, *J. Hazard. Mater.*, 2020, **383**, 121123.

21 H. Amid, B. Maze, M. C. Flickinger and B. Pourdeyhimi, Hybrid adsorbent nonwoven structures: A review of current technologies, *J. Mater. Sci.*, 2016, **51**, 4173–4200.

22 N. H. Elsayed, R. A. S. Alatawi, O. H. N. Alhawiti, I. S. Elashmawi, A. Alatawi and A. H. Al-Marri, Polyaniline grafted melt-spun PET fibers for anionic dye removal, *Desalin. Water Treat.*, 2020, **195**, 334–340.

23 S. Wang, A. Lu and L. N. Zhang, Recent advances in regenerated cellulose materials, *Prog. Polym. Sci.*, 2016, **53**, 169–206.

24 S. K. Ramamoorthy, M. Skrifvars and A. Persson, A review of natural fibers used in biocomposites: Plant, animal and regenerated cellulose fibers, *Polym. Rev.*, 2015, **55**, 107–162.

25 K. He, G. M. Zeng, A. W. Chen, Z. Z. Huang, M. Peng, T. T. Huang and G. Q. Chen, Graphene hybridized polydopamine-kaolin composite as effective adsorbent for methylene blue removal, *Composites, Part B*, 2019, **161**, 141–149.

26 M. O. Mavukkandy, Y. Ibrahim, F. Almarzooqi, V. Naddeo, G. N. Karanikolos, E. Alhseinat, F. Banat and S. W. Hasan, Synthesis of polydopamine coated tungsten oxide@ poly(vinylidene fluoride-co-hexafluoropropylene) electrospun nanofibers as multifunctional membranes for water applications, *Chem. Eng. J.*, 2021, **427**, 131021.

27 J. Lee, J. Y. Moon, J. C. Lee, T. I. Hwang, C. H. Park and C. S. Kim, Simple conversion of 3D electrospun nanofibrous cellulose acetate into a mechanically robust nanocomposite cellulose/calcium scaffold, *Carbohyd. Polym.*, 2021, **253**, 117191.

28 S. Rella, E. Mazzotta, A. Caroli, M. D. Luca, C. Bucci and C. Malitesta, Investigation of polydopamine coatings by X-ray Photoelectron Spectroscopy as an effective tool for improving biomolecule conjugation, *Appl. Surf. Sci.*, 2018, **447**, 31–39.

29 P. M. Cuesta Zapata, J. F. Miranda, F. Orellana, E. Gonzo and N. A. Bonini, Synthesis of Cu/SiO$_2$(MCM-41) mesostructured catalysts. Effect of the preparation method on the textural properties and chemical structure, *Mater. Chem. Phys.*, 2022, **287**, 126232.

30 S. E. Moradi, Microwave assisted preparation of sodium dodecyl sulphate (SDS) modified ordered nanoporous carbon and its adsorption for MB dye, *J. Ind. Eng. Chem.*, 2014, **20**, 208–215.

31 Q. X. Fu, Y. Si, L. F. Liu, J. Y. Yu and B. Ding, Elaborate design of ethylene vinyl alcohol (EVAL) nanofiber-based chromatographic media for highly efficient adsorption and extraction of proteins, *J. Colloid Interf. Sci.*, 2019, **555**, 11–21.

32 Y. Zou, J. Y. Zhao, J. Y. Zhu, X. Y. Guo, P. Chen, G. G. Duan, X. H. Liu and Y. W. Li, A mussel-inspired polydopamine-filled cellulose aerogel for solar-enabled water remediation, *ACS Appl. Mater. Interfaces*, 2021, **13**, 7617–7624.

33 S. Jia, D. Tang, Y. Zhou, Y. Du, J. Peng, Z. Sun and X. Yang, Polydopamine microsphere-incorporated electrospun fibers as novel adsorbents for dual-responsive adsorption of methylene blue, *ACS Appl. Mater. Interfaces*, 2020, **12**, 7617–7624.

34 C. R. Wang, J. J. Yin, R. Wang, T. F. Jiao, H. M. Huang, J. X. Zhou, L. X. Zhang and Q. M. Peng, Facile preparation of self-assembled polydopamine-modified electrospun fibers for highly effective removal of organic dyes, *Nanomaterials*, 2019, **9**, 116.

35 L. H. Chen, W. P. Hsu, H. W. Chan and Y. L. Lee, Fabrication of P3HT/gold nanoparticle LB films by P3HT templating Langmuir monolayer, *Appl. Surf. Sci.*, 2014, **320**, 736–741.

36 P. P. Chen, H. P. Zhang, J. P. Ding, X. Y. Lin, X. Lu, C. S. Liu and Y. H. Tang, Carboxylmethyl konjac glucomannan conjugated polydopamine composites for Pb(II) removal, *Carbohyd. Polym.*, 2017, **162**, 62–70.

37 P. Benjwal, R. Sharma and K. K. Kar, Effects of surface microstructure and chemical state of feather fiber-derived multidoped carbon fibers on the adsorption of organic water pollutants, *Mater. Design*, 2016, **110**, 762–774.

38 P. F. Erica, S. S. Társila, M. C. Cenira, S. Rangabhashiyam, C. Nhamo, M. T. M. O. Leonardo, M. P. M. Simoni and M. Lucas, Efficient adsorption of dyes by γ-alumina synthesized from aluminum wastes: Kinetics, isotherms, thermodynamics and toxicity assessment, *J. Environ. Chem. Eng.*, 2021, **9**, 106198.

39 Z. H. Ding, X. Hu, A. R. Zimmerman and B. Gao, Sorption and cosorption of lead (II) and methylene blue on chemically modified biomass, *Bioresource Technol.*, 2014, **167**, 569–573.

40 Y. Q. Jin, C. M. Zeng, Q. F. Lü and Y. Yu, Efficient adsorption of methylene blue and lead ions in aqueous solutions by 5-sulfosalicylic acid modified lignin, *Int. J. Biol. Macromol.*, 2019, **123**, 50–58.

41 H. R. Shan, X. Q. Wang, F. H. Shi, J. H. Yan, J. Y. Yu and B. Ding, Hierarchical porous structured SiO$_2$/SnO$_2$ nanofibrous membrane with superb flexibility for molecular filtration, *ACS Appl. Mater. Interfaces*, 2017, **9**, 18966–18976.

42 L. Li, H. R. Ren, Y. L. Liu, Y. X. Zhao, X. H. Zhou, W. M. Kang, X. P. Zhuang and B. W. Cheng, Facile construction of hierarchical porous ultrafine alumina fibers (HPAFs) and its application for dye adsorption, *Microporous Mesoporous Mater.*, 2020, **308**, 110544.

43 L. Meng, X. H. Xu, B. Bai, M. L. Ma, S. Li, N. Hu, H. L. Wang and Y. R. Suo, Surface carboxyl-activated polyester (PET) fibers decorated with glucose carbon microspheres and their enhanced selective adsorption for dyes – ScienceDirect, *J. Phys. Chem. Solids*, 2018, **123**, 378–388.

44 D. K. Mahmoud, M. A. M. Salleh, W. A. W. A. Karim, A. Idris and Z. Z. Abidin, Batch adsorption of basic dye using acid treated kenaf fibre char: Equilibrium, kinetic and thermodynamic studies, *Chem. Eng. J.*, 2012, **181**, 449–457.

45 H. Demir, A. Top, D. Balköse and S. Ülkü, Dye adsorption behavior of Luffa cylindrica fibers, *J. Hazard. Mater.*, 2008, **153**, 389–394.

46 H. Chakhtouna, N. Zari, R. Bouhfid, A. E. K. Qaiss and H. Benzeid, Novel photocatalyst based on date palm fibers for efficient dyes removal, *J. Water Process Eng.*, 2021, **43**, 102167.

47 R. Krishnamoorthi, R. Anbazhagan, H. C. Tsai, C. F. Wang and J. Y. Lai, Biodegradable, superwettable caffeic acid/chitosan polymer coated cotton fibers for the simultaneous removal of oils, dyes, and metal ions from water, *Chem. Eng. J.*, 2022, **427**, 131920.

48 J. Li, S. S. Yuan, J. Y. Zhu and B. V. D. Bruggen, High-flux, antibacterial composite membranes *via* polydopamine-assisted PEI-TiO$_2$/Ag modification for dye removal, *Chem. Eng. J.*, 2019, **372**, 275–284.

49 Q. Shi, J. Q. Meng, R. S. Xu, X. L. Du and Y. F. Zhang, Synthesis of hydrophilic polysulfone membranes having antifouling and boron adsorption properties *via* blending with an amphiphilic graft glycopolymer, *J. Membrane Sci.*, 2013, **444**, 50–59.

50 S. Y. Shi, C. H. Xu, X. Q. Wang, Y. S. Xie, Y. P. Wang, Q. Dong, L. Y. Zhu, G. H. Zhang and D. Xu, Electrospinning fabrication of flexible Fe$_3$O$_4$ fibers by sol-gel method with high saturation magnetization for heavy metal adsorption, *Mater. Design*, 2020, **186**, 108298.

51 Z. W. Ma, M. Kotaki and S. Ramakrishna, Electrospun cellulose nanofiber as affinity membrane, *J. Membrane Sci.*, 2005, **265**, 115–123.

52 Y. M. Chen, S. J. Li, X. L. Li, C. T. Mei, J. J. Zheng, E. Shiju, G. G. Duan, K. M. Liu and S. H. Jiang, Liquid transport and real-time dye purification *via* lotus petiole-inspired long-range-ordered anisotropic cellulose nanofibril aerogels, *ACS Nano*, 2022, **15**, 20666–20677.

53 Y. Wu, M. Gao, W. Chen, Z. Lü and C. Gao, Efficient removal of anionic dye by constructing thin-film composite membrane with high perm-selectivity and improved anti-dye-deposition property, *Desalination*, 2020, **476**, 114228.